



## Article

# Wind Simulations over Western Patagonia Using the Weather Research and Forecasting Model and Reanalysis

Hugo Vásquez Anacona <sup>1</sup>, Cristian Mattar <sup>2,\*</sup>, Nicolás G. Alonso-de-Linaje <sup>3</sup> , Héctor H. Sepúlveda <sup>4,5</sup>  and Jessica Crisóstomo <sup>6</sup>

<sup>1</sup> Laboratory of Analysis of the Biosphere (LAB), University of Chile, Santiago 8320000, Chile; hugo.vasquez@ug.uchile.cl

<sup>2</sup> Fundación Bioera, Santiago 8320000, Chile

<sup>3</sup> DTU Wind and Energy Systems, 4000 Roskilde, Denmark; nicdel@dtu.dk

<sup>4</sup> Department of Geophysics (DGEO), University of Concepcion, Concepción 4030000, Chile; andres@dgeo.udec.cl

<sup>5</sup> Fundación CEQUA, Punta Arenas 6200000, Chile

<sup>6</sup> Servicio Meteorológico de la Armada de Chile, Valparaíso 2340000, Chile; jcrisostomo@dgtm.cl

\* Correspondence: cmattar@uchile.cl

**Abstract:** The Chilean Western Patagonia has the highest wind potential resources in South America. Its complex terrain deserves a special attention for wind modeling and assessments. In this work, we have performed a comprehensive meso-scale climate simulation on Weather Research and Forecasting (WRF) in order to provide new insights into the wind climatology in Western Patagonia. Simulations were carried out from 1989 to 2020, and we considered a previous sensitivity analysis for their configuration. In situ data from a wind mast, meteorological information and data from eddy flux stations were used to evaluate the results. Reanalysis data from ERA-5, MERRA-2 and RECON80-17 were also used to perform a comparison of the obtained results with the WRF simulation. The results show that the WRF simulation using ERA-5 presented in this work is slightly different to a mathematical reconstruction using MERRA-2 (RECON80-17), which is widely accepted in Chile for wind resource assessments, presenting a statistical difference of about  $EMD = 0.8 [m s^{-1}]$  and  $RMSE = 0.5$ . Non-significative differences were found between the WRF simulation and MERRA-2 reanalysis, while ERA-5 with MERRA-2 presented a remarkable statistical difference of about  $EMD = 1.64 [m s^{-1}]$  and  $RMSE = 1.8$ . In relation to flux comparison, reanalysis and WRF in contrast with in situ observations presented a good performance during the summer season, although a spatial resolution bias was noticed. These results can be used as an input for further research related to WRF simulations in Western Patagonia to provide reliable information on wind energy exploration and extreme climatological phenomena such as heat waves.

**Keywords:** WRF; forecast; reanalysis; Western Patagonia; wind climate; Chile



**Citation:** Vásquez Anacona, H.; Mattar, C.; G. Alonso-de-Linaje, N.; Sepúlveda, H.H.; Crisóstomo, J. Wind Simulations over Western Patagonia Using the Weather Research and Forecasting Model and Reanalysis. *Atmosphere* **2023**, *14*, 1062. <https://doi.org/10.3390/atmos14071062>

Academic Editors:

Edoardo Bucchignani and Andrea Mastellone

Received: 6 May 2023

Revised: 10 June 2023

Accepted: 20 June 2023

Published: 23 June 2023



**Copyright:** © 2023 by the authors. Licensee MDPI, Basel, Switzerland. This article is an open access article distributed under the terms and conditions of the Creative Commons Attribution (CC BY) license (<https://creativecommons.org/licenses/by/4.0/>).

## 1. Introduction

Observational measurements in Western Patagonia (WP) are critical for exploring new topics in climate sciences and wind climate patterns. The area of WP goes from 43 to 50° S and 71 to 76° W, including complex terrain areas, fjords, canals, estuaries, peninsulas, isthmuses and mountains [1]. The spatial scarcity of in situ measurements deserves special attention because new insights into climate change must be compared with ground truth observations in order to determine the magnitude and differences between several data sources. Indeed, the inputs for climate assessment and current climate change deserve new techniques to analyze water regimes and extreme events in WP and possible consequences [2–4]. In this context, the use of models such as Weather Research and Forecasting (WRF) is an alternative to fill the spatial and temporal gaps from observational data and to present new approaches for climate assessments.

WRF is a widely used numerical weather prediction system that offers high-resolution simulations, regional and global coverage, and the ability to represent various physical processes, such as atmospheric dynamics, radiation, and microphysics. The model needs to be initialized using initial meteorological conditions which can be provided by reanalysis data sets such as Global Forecast System (GFS), ERA-Interim and ERA-5 [5–7]. These data sources provide a physically consistent representation of the atmosphere at a global scale [8]. One commonly used source of wind data is ERA5 reanalysis, which has been found to be reliable for wind resource assessment applications in offshore environments, as demonstrated by [9–12]. ERA5 is the fifth-generation and the most updated (2019) global reanalysis product developed by the European Centre for Medium-Range Weather Forecast (ECMWF) within the Copernicus Climate Change Service (CDS). Furthermore, ERA5 reanalysis is an upgraded version of its predecessor, ERA-Interim, as it offers a higher temporal resolution of 1 h, a finer spatial resolution of ~31 km and wind data available at 100 m height. Among all global reanalysis products with a 1 h temporal resolution, ERA5 has the highest spatial resolution and wind height [12]. Another reanalysis that is highly resolved in time and space and used for wind power generation is MERRA version 2 [13,14]. MERRA2 reanalysis is the improved successor of MERRA, both produced by NASA and commonly used for climatological studies at country and regional scales. This data set has been widely used due to the hourly temporal resolution, the  $0.5^\circ \times 0.625^\circ$  spatial resolution and a height of 50 m for wind speed. However, it is important to note that the accuracies of these data sets depend on the availability of in situ data and the features of the terrain. In particular, [12] found that ERA5 reanalysis showed good performance in predicting wind speed in flat and homogeneous areas such as FINO3 (Germany) and Cabauw (Netherlands), with 95–96% and 93–94% correlation coefficients, respectively. However, over complex terrain characterized by mountains and forests, such as Boulder (US) and Ghoroghchi (Iran), the ERA5 wind speed magnitude and variation were found to be significantly biased, with a correlation coefficient of 38 and 47%, respectively. Similarly, MERRA2 reanalysis showed more errors in representing surface wind fields in areas with more varying and complex land–sea topography and coastal areas [15]. Additionally, the use of reanalysis can present some bias according to the nudging, the relief, and land cover, among others [16–19].

Ref. [20] conducted a study in which they compared climatic data from multiple sources, including MERRA-2, ERA-5, and GLDS, with data from two meteorological stations. However, the presence of noise and flagged information near coastal areas and fjords can limit its accuracy in assessing wind resources in these regions. Thus, there is a need to implement a new calibration model for austral zones, in particular WP, using the combination of reanalysis and in situ and numerical simulations as an alternative to wind climate assessment.

Despite the important advances in scientific knowledge and climate dynamics over WP, wind resource assessment remains partially explored because it is a complex area of study with few observational sites. For instance, there is a single wind field station (Melinka Island) per 1.200 km<sup>2</sup> in the vast area covering the Penas Gulf and the surroundings of the Moraleda Channel, limiting the knowledge at local scales and creating a lack of information related to wind field dynamics in the region. Thus, it is necessary to address this topic in terms of a better understanding of the existing Ocean–Land–Atmosphere interaction (i.e., at better spatial resolution) and initial conditions in forecast models for Western Patagonia. The aim of this work is thus to generate a new wind climatology for Western Patagonia in order to analyze the existing climate trends over the region by using reanalysis and numerical simulations. The manuscript is structured as follows: Section 2 introduces the study area, Section 3 outlines the data and methods used, Section 4 presents the key findings of the study, and Sections 5 and 6 provide the discussion and conclusion, respectively.

## 2. Study Area

The study area covers Western Patagonia in the Aysén region of Chile. This area is characterized by a high amount of precipitation (>3000 mm per year) and several fjords and islands. The Taitao peninsula is the most iconic geographical location where the Humboldt current arises from the western Pacific Ocean, carrying cold waters and very high wind fields. The Moraleda Channel is located in the middle of this region, separating the island and the continental strip, which is characterized by several fjords. More than 50% of the study area is part of the National Park system, and several aquaculture areas are located in this area. The wind patterns in WP are significantly impacted by the local topography and unique environmental conditions. Near coastal areas, the mean wind speeds are approximately  $4 \text{ m s}^{-1}$  and  $7 \text{ m s}^{-1}$  at the Ad. Melinka and Melinka Repollal stations, respectively. These areas experience a predominantly south-west wind direction, which tends to remain stable throughout the seasons. Inside fjords, the mean values are quite a bit lower, reaching a value of  $2.3 \text{ m s}^{-1}$  according to the PFA station with the same predominant wind direction. On the surface of the land, such as in valleys, the wind speeds tend to be higher. The Mirador Marchant and Puesto Viejo stations report average wind speeds of  $6.5 \text{ m s}^{-1}$  and  $7.3 \text{ m s}^{-1}$ , respectively. These locations also exhibit a similar south-west wind direction as the prevailing pattern and are more sensible to seasonal change through an annual period. Summer and spring exhibit maximum wind speeds exceeding  $18 \text{ m s}^{-1}$  in the region.

In this study area, one mast was installed in the Aysén Fjord, which was a 10 m fixed mast including two Vector anemometers for wind speed, which were installed at 2.5 and 5 m heights, and one Marine R.M. A Young anemometer and vane were installed at 10 m. To assess temperature and relative humidity, a barometer and one solar radiation sensor were also installed. These instruments were connected to a data logger (CR1000X), and the parameters were measured at 1 min, and the averages were recorded every 5 min.

## 3. Data and Methodology

### 3.1. Meteorological Stations

All measurement stations are located onshore and were used to evaluate the model simulation outputs separately due to different measurement periods (see Table 1 for details). The distribution of the measurement stations is depicted in Figure 1. The stations are equipped with sensors to measure various atmospheric variables, such as wind speed and direction, temperature, humidity and radiation. These measurements provide valuable data on local atmospheric conditions and are used to validate the model simulations.

**Table 1.** Meteorological mast sites used in the wind speed comparison.

Station Name	Altitude (m)	Height (m.a.g.l)	Start Date	End Date	Data Source
Melinka repollal	100	34.6	12 November 2010	2 December 2011	Wind explorer
Puesto viejo	850	20	25 February 2004	18 May 2005	Wind explorer
Islas las huichas	101	20	22 June 2005	9 August 2006	Wind explorer
Ad. Melinka	8	10	1 January 2014	1 January 2020	Meteochile
Ad. Puerto Aysén	11	10	1 January 1960	1 January 2020	Meteochile
Ad. Teniente Vidal	299	10	1 January 1946	1 January 2020	Meteochile
Cisnes Puyuhuapi	11	10	1 January 2016	1 January 2020	Meteochile
Mirador Marchant	480	10	11 January 2019	1 February 2020	Meteochile
Villa O'Higgins	280	10	1 January 2013	1 January 2020	Meteochile
PFA (Fjord Aysen)	5	2, 5, 10	11 January 2020	14 February 2020	F. 1,181,155

### 3.2. Eddy Covariance Flux Tower

The Ñirehuao flux tower ( $45.241353^\circ \text{ S}$ ,  $71.796942^\circ \text{ W}$ ) is equipped with an advanced Eddy Covariance (EC) measurement system based on an open-path gas analyzer and a three-dimensional sonic anemometer–thermometer (IRGASON, Campbell Scientific, Logan, UT, USA), and it was used in this work. Other meteorological instruments included in the tower are CNR-4 for net radiation (Kipp & Zonen, The Netherlands); instruments to

determine snow depth (SR50, CSI, Bohemia, NY, USA), the air temperature and relative humidity (HMP60, Vaisala, Finland), the surface temperature (SI-411, Apogee, Logan, UT, USA), the soil moisture and temperature (CS655L12, CSI, Bohemia, NY, USA), rainfall (Texas Inc., Dallas, TX, USA), wind measurements and directions (Young Inc.); and a ground flux plate (Hukseflux Inc., The Netherlands). To quality check and correct fluxes of sensible and latent heat, the EasyFlux DL software from Campbell Scientific (more details available at: <https://www.campbellsci.com/easyflux-dl>, accessed on 20 March 2023) was used to process the raw data collected by the datalogger. The sensor was positioned at a height of 2.5 m during the period of 25 December 2019 to 4 February 2020, and the data were continuously collected and monitored using a datalogger (Campbell Scientific, CR3000).

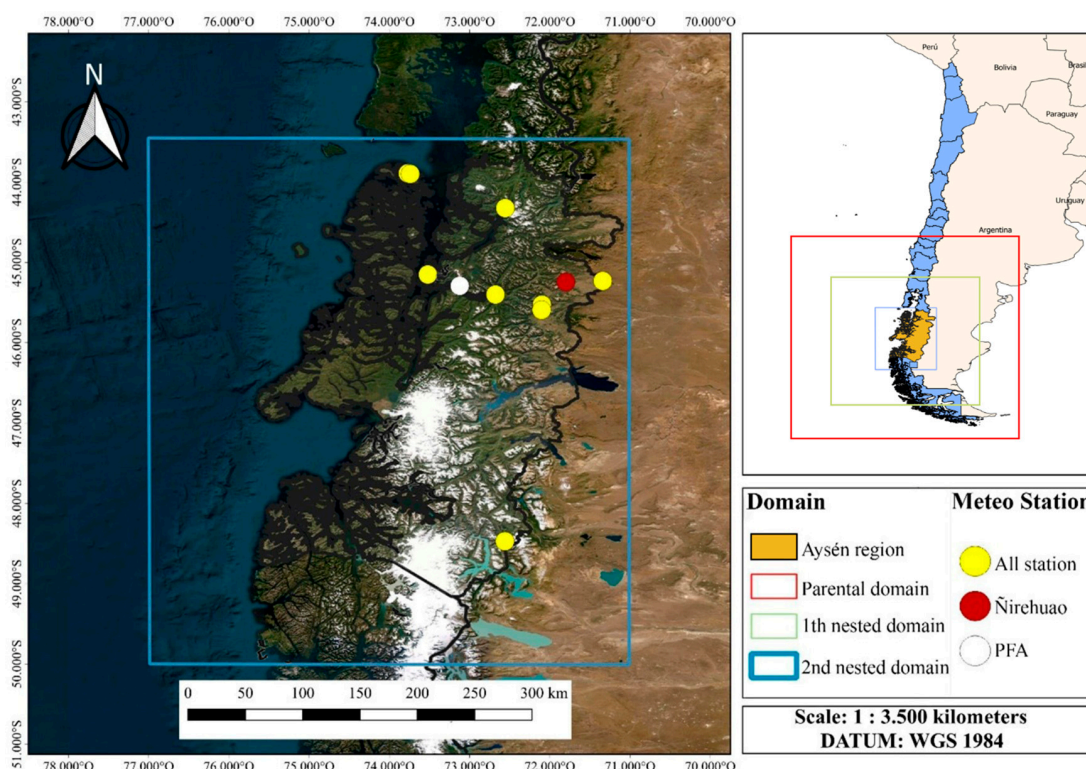


**Figure 1.** Study area, simulation domains and location of several in situ data points.

### 3.3. Wind Speed Data Sets

In this study, five wind speed data sets are evaluated (see Table 2). Two global reanalysis tools, ERA-5 and MERRA-2, were selected due to their consistency in climatological studies, as well as the mathematical reconstruction RECON80-17 produced by [6] and a Numerical Weather Prediction (NWP) simulation based on the Weather Research and Forecasting (WRF) model forced by ERA5 (more details in Section 3.3), called WRF\_E5 here.

**Table 2.** Information on the numerical data sets evaluated in the study.

Option	MERRA-2	ERA-5	WRF_E5	RECON80-17
Institution	NASA GMAO	ECMWF	-	MinEnergia
Model	GEOS v5.12.4	IFS Cycle 41r2	WRF v3.7.1	Mathematical reconstruction
Spatial coverage	Global	Global	Western Patagonia	Chile
Boundary condition	-	-	ERA-5	MERRA-2
Data assimilation	3D-Var	4D-Var	Nudging	-
Horizontal grid spacing	0.5° × 0.625°	0.25°	3 km	1 km
Vertical wind speed heights (m)	10, 50	10, 100	10	5.5–180
Time coverage	1980–present	1979–present	1980–2020	1980–2017
Time resolution	1 h	1 h	1 h	1 h

### 3.4. Mesoscale Simulation

The mesoscale wind fields were modeled by applying WRF version 3.7.1. This is a widely used state-of-the-art NWP (Numerical Weather Prediction) modeling code developed by the NCEP (National Center for Environmental Prediction) and the National Center for Atmospheric Research (NCAR), among other institutions. The WRF model is a three-dimensional, non-hydrostatic model widely used among the scientific community for atmospheric research, weather forecasting and industry applications. A detailed explanation of this model can be found in [21].

The study area's initial and boundary conditions were obtained from the ERA-5 reanalysis at 1 h intervals. To simulate offshore wind fields, a configuration was adopted from the analysis performed by [7]. The configuration includes three nested domains with 27, 9 and 3 km of spatial resolution for the main domain, nested domain 1 and nested domain 2, respectively (Figure 1). The two-way nesting domain configuration was implemented to ensure information exchange among the three domains. To prevent values of variables like the U and V wind components from deviating from the reanalysis data, the spectral nudging technique was employed. Table 3 outlines the physical configuration used in the simulation.

**Table 3.** Configuration of physical parameters of WRF.

Parameterization	Option
PBL	MYNN 2.5
SL	MYNN
LSM	Noah-LSM
Microphysics	WSM 5
Cumulus	Kain-Fritsch
LWR	RRTMG
SWR	Dudhia

This parameterization is derived from a previous sensitivity analysis conducted in Chile [7], which demonstrated excellent agreement with observations in coastal regions. Furthermore, the MYNN 2.5 planetary boundary layer (PBL) scheme has been widely validated and recognized as highly versatile for various terrains, including both flat and complex topographies. As a result, it has been extensively utilized in other wind atlases such as the New European Wind Atlas [22] and the Wind Atlas of South Africa [23].

Nested domain 2 was specifically designed to cover the area of interest, with its center located at latitude 46.133405 S and longitude 73.491219 W. The simulation period for this domain spanned from 1 January 1980 to 31 December 2020. Each simulation was initialized at 0000UTC and ran for a period of 10 days, with the first 24 h designated as a model spin-up period to allow for the model to stabilize and produce accurate results. Finally, the default WRF 3.7.1 land use configuration USGS was used to provide land-use characteristics such as static fields of topography, land–water masks, land use/cover classification, albedo and emissivity, among others. This product has a horizontal spatial resolution of 10 min, 2 min and 30 s for parental, nested domain 2 and nested domain 1, respectively and 24 categories of land use for each of them.

### 3.5. Statistical Analysis

The wind speed was evaluated in terms of its distribution given by the Weibull method. It estimates the probability curve for the occurrence of simulated wind speeds and determines the shape and scale factors through the method of least squares. The Weibull parameters were obtained by assuming an air density of 1.225 kg/m<sup>3</sup>.

$$P(v) = \left(\frac{\beta}{\alpha}\right) \times \left(\frac{v}{\alpha}\right)^{\beta-1} \times e^{-\left(\frac{v}{\alpha}\right)^{\beta}}$$

where  $P(v)$  corresponds to the Weibull occurrence probability ( $-$ ),  $\bar{V}$  is the simulated wind speed ( $m/s^{-1}$ ),  $\alpha$  is the scale factor and  $\beta$  is the shape factor of the Weibull distribution ( $-$ ).

The Earth mover’s distance (EMD), also known as the Wasserstein distance, is a computational technique that was first introduced by [24] in computer science studies and recently applied by [22] for wind resource assessment studies. The EMD is defined by the area between two cumulative density functions (CDFs) and, therefore, is always positive. This technique has proven to be useful in assessing the accuracy of wind speed distribution simulations by quantifying the difference between simulated and observed wind speed distributions [25].

The RMSE is a metric that measures the difference between the predicted values and the observed values and shows the mean magnitude of this error.

$$RMSE = \sqrt{\left(\frac{1}{N} \sum_{i=1}^n (X_i - Y_i)\right)^2}$$

where “ $n$ ” corresponds to the number of observations, “ $X_i$ ” corresponds to the estimated value and “ $Y_i$ ” corresponds to the observed value.

#### 4. Results and Analysis

##### 4.1. Comparison of Wind Speed from ERA-5, MERRA-2, RECON80-17 and WRF\_E5 Simulation

The accuracy of the thirty-year WRF simulation (WRF\_E5), RECON80-17, ERA-5 and MERRA-2 reanalysis in reproducing wind speed patterns was evaluated by using statistical metrics such as RMSE and EMD. The climatological reconstruction referred to here as RECON80-17 was used for comparison with the WRF\_E5 simulation. Due to the time period availability of RECON80-17 and the meteorological stations, it was only used for three measurement sites in the study area: Islas Las Huichas, Melinka Repollal and Puesto Viejo. Table 4 presents the results for each measurement station and an average station to assess the overall performance. The data sets with the best performance for each metric are highlighted in bold.

**Table 4.** Values of EMD and RMSE for WRF\_E5, ERA-5 and MERRA-2 in all stations.

Measurement Sites	Data	RMSE m s <sup>-1</sup>	EMD m s <sup>-1</sup>
PFA	WRF_E5	2.6	1.28
	ERA-5	4.8	3.60
	MERRA-2	<b>1.6</b>	<b>0.23</b>
	RECON80-17	-	-
Ad. Melinka	WRF_E5	<b>2.3</b>	<b>0.64</b>
	ERA-5	4.1	1.60
	MERRA-2	3.2	1.52
Mirador Marchant	RECON80-17	-	-
	WRF_E5	<b>4.3</b>	2.65
	ERA-5	4.7	<b>1.02</b>
	MERRA-2	4.4	3.10
Villa O’Higgins	RECON80-17	-	-
	WRF_E5	<b>2.6</b>	<b>1.08</b>
	ERA-5	4.82	3.27
	MERRA-2	4.71	3.65
Puerto Aysén	RECON80-17	-	-
	WRF_E5	2.1	0.62
	ERA-5	5.0	3.58
	MERRA-2	<b>1.8</b>	<b>0.53</b>
	RECON80-17	-	-

Table 4. Cont.

Measurement Sites	Data	RMSE m s <sup>-1</sup>	EMD m s <sup>-1</sup>
Cisnes Puyuhuapi	WRF_E5	2.2	<b>0.78</b>
	ERA-5	5.9	4.87
	MERRA-2	<b>1.7</b>	0.82
	RECON80-17	-	-
Ad. Teniente Vidal	WRF_E5	<b>1.7</b>	<b>0.33</b>
	ERA-5	4.8	3.60
	MERRA-2	2.1	1.14
	RECON80-17	-	-
Islas las Huichas	WRF_E5	4.8	1.91
	ERA-5	<b>4.4</b>	1.89
	MERRA-2	4.5	2.19
	RECON80-17	4.5	<b>1.21</b>
Melinka Repollal	WRF_E5	3.3	2.49
	ERA-5	4.3	3.45
	MERRA-2	2.4	<b>0.31</b>
	RECON80-17	<b>2.1</b>	1.16
Puesto Viejo	WRF_E5	3.1	0.86
	ERA-5	4.1	2.23
	MERRA-2	3.6	0.71
	RECON80-17	<b>3.1</b>	<b>0.46</b>

The analysis of WRF\_E5 and RECON80-17 was applied to the three stations where the climatological reconstruction has available data. Based on these data, RECON80-17 had the best performance with 0.94 m s<sup>-1</sup> in EMD and 3.2 m s<sup>-1</sup> for RMSE. The WRF\_E5 presented small differences in relation to the climatological reconstruction, with a difference of 0.81 m s<sup>-1</sup> for EMD and 0.5 m s<sup>-1</sup> in RMSE in the average station. In this sense, the RECON80-17 data set was proven to be the most effective option for predicting wind speeds patterns at these stations, except for the Melinka Repollal station.

On the other hand, the best performance in terms of EMD and RMSE was given by MERRA-2, with a remarkable difference in contrast with ERA-5, with values of 1.64 m s<sup>-1</sup> for EMD and 1.8 m s<sup>-1</sup> for RMSE. In the case of the Mirador Marchant station, the ERA-5 reanalysis had the best performance. On the other hand, the comparison between WRF\_E5 and MERRA-2 metric values revealed a small difference of 0.05 m s<sup>-1</sup> in terms of EMD and no difference in RMSE for the average station.

The ERA-5 reanalysis had poor performance in the study area, as can be seen in Table 4. Despite the poor performance of this reanalysis, applying the WRF model simulation to this data set resulted in significant changes to the average values (ERA-5 to WRF\_E5). Specifically, there was a reduction of 1.59 m s<sup>-1</sup> in EMD and a reduction of 1.7 m s<sup>-1</sup> in RMSE. The only instances where the use of the WRF model simulation resulted in a decrease in overall performance were at the Mirador Marchant station, with an increase of 1.63 for EMD and a decrease of 0.4 m s<sup>-1</sup> for RMSE, and in the Islas las Huichas measurement station, where there was an insignificant increase in EMD and a decrease of 0.4 m s<sup>-1</sup> for RMSE. Despite this obtained effect at these stations, the application of the WRF model over ERA-5 reanalysis in this complex terrain offers a clear advantage in most of the measurement stations by enabling the incorporation of a higher level of detail about the land use, topography and air roughness of the study area. This level of detail is particularly valuable in the analysis of wind resources due to the complexity of the terrain, as it allows for a more accurate and comprehensive understanding of the local-scale wind conditions.

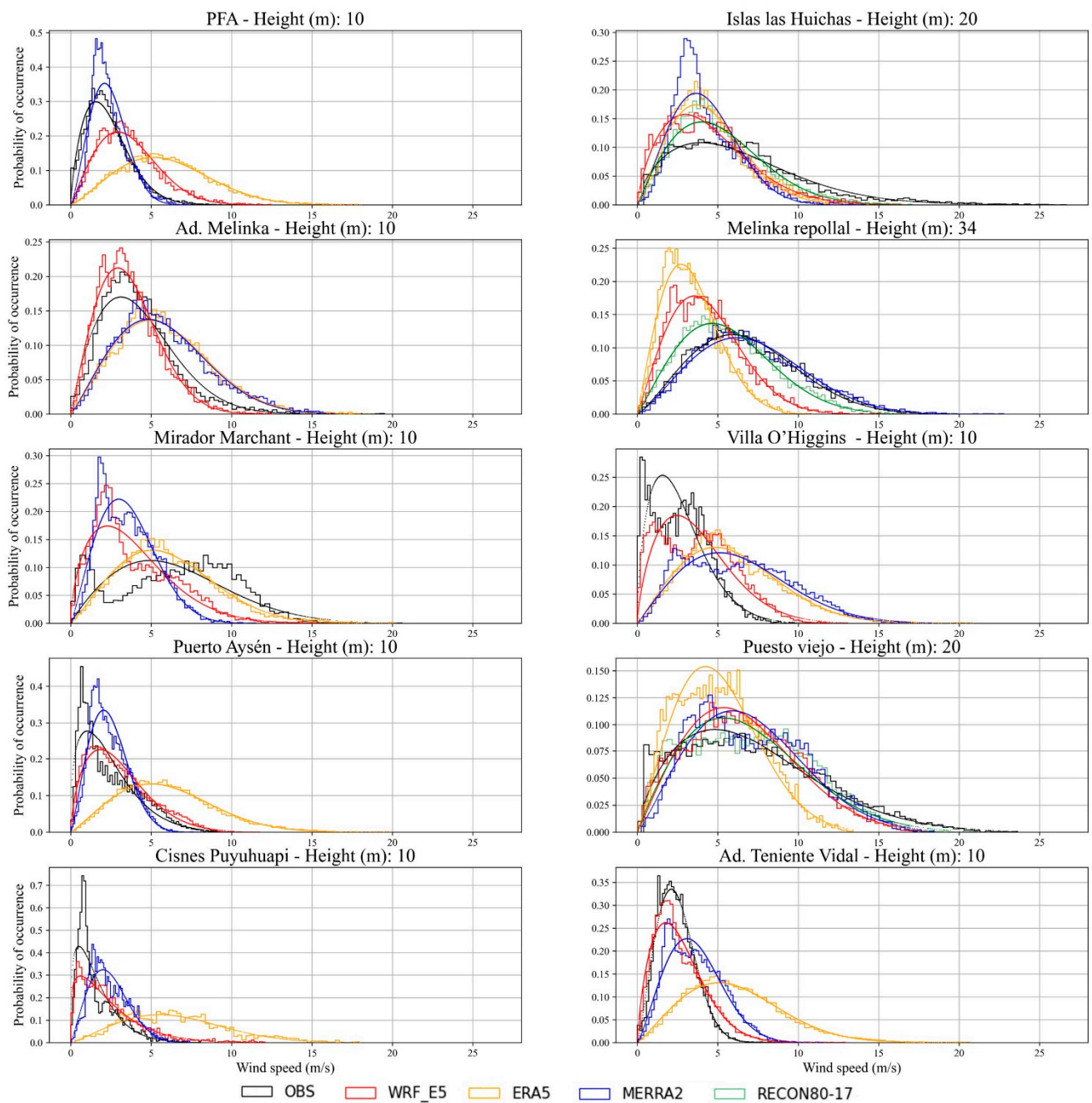
Figure 2 shows the Weibull Probability Density Function (PDF) curves and histograms for wind speed at all the stations. At the PFA station, the wind speed distribution for the full range of values (0–7 m s<sup>-1</sup>) is only fitted for MERRA-2 reanalysis, presenting a difference of 5% of probability of occurrence at 2.5 m s<sup>-1</sup>, where the rest of data sets present differences higher than 10%. Therefore, is important to note that the wind speed observa-

tions higher than  $5 \text{ m s}^{-1}$  accounted for just 4% of the wind speed values, while WRF\_E5 and ERA-5 increased the probability of occurrence at this point, accounting for over 20% of data. For the Ad Melinka station, the wind distribution presented the same range of wind speed ( $0\text{--}10 \text{ m s}^{-1}$ ) for all data sets, although there was a difference at  $2.5 \text{ m s}^{-1}$ , where the observation presented a maximum of 18%, which is closely shared by WRF\_E5 with a value of 20%; the rest of data sets presented decreased probabilities of occurrence, leading to an overprediction of wind speed values higher than  $7 \text{ m s}^{-1}$  as a result. At the Mirador Marchant station, there was a clear fit with ERA-5 reanalysis, sharing the same range of wind speed values ( $0\text{--}15 \text{ m s}^{-1}$ ), while WRF\_E5 and MERRA-2 exhibited a smaller range ( $0\text{--}10 \text{ m s}^{-1}$ ), obtaining increased probabilities of occurrence over 18% at  $2.5 \text{ m s}^{-1}$  as a result, where the observations presented a maximum of 10%, and decreased probabilities of occurrence under 5% at wind speeds higher than  $7 \text{ m s}^{-1}$ , where observations presented a maximum of 10% as well. As a result, the 15% of data gathered at observed wind speeds higher than  $10 \text{ m s}^{-1}$  were not present at these two data sets. At the Villa O'Higgins station, the wind distribution presented the same range of wind speed values ( $0\text{--}10 \text{ m s}^{-1}$ ) as for WRF\_E5, while for the rest of the data sets, this range was higher ( $0\text{--}15 \text{ m s}^{-1}$ ) and led to increased probabilities of occurrence at higher wind speed values over  $5 \text{ m s}^{-1}$ . It is important to note that the observed wind distribution at  $5 \text{ m s}^{-1}$  gathered 15% of data, while the rest of the data sets gathered over 20%, and specifically, ERA-5 and MERRA-2 gathered more than 40% of data at this point, clearly overpredicting wind speed values. At the Puerto Aysén and Cisnes Puyuhuapi stations, the wind distributions were characterized by low wind speed values ranging from 0 to  $10 \text{ m s}^{-1}$  and had a peak at  $2 \text{ m s}^{-1}$  with maximum probabilities of occurrences of 27 and 42% for Puerto Aysén and Cisnes Puyuhuapi, respectively. For Puerto Aysén, all data sets presented the same range of wind distribution, except ERA-5, which had higher wind speed values ( $0\text{--}15 \text{ m s}^{-1}$ ). All data sets tended to decrease below 20% of the probability of occurrence at the peak of observed wind distribution. Meanwhile, for the Cisnes Puyuhuapi station, WRF\_E5 and MERRA-2 exhibited the same range of wind speed values in the wind distribution ( $0\text{--}7 \text{ m s}^{-1}$ ), but there was also a difference at the observed peak, where all data sets presented a decrease in their probability of occurrence below 32%. It can be noted that at this point, the observations gathered 72% of data, while other data sets gathered less than 60%.

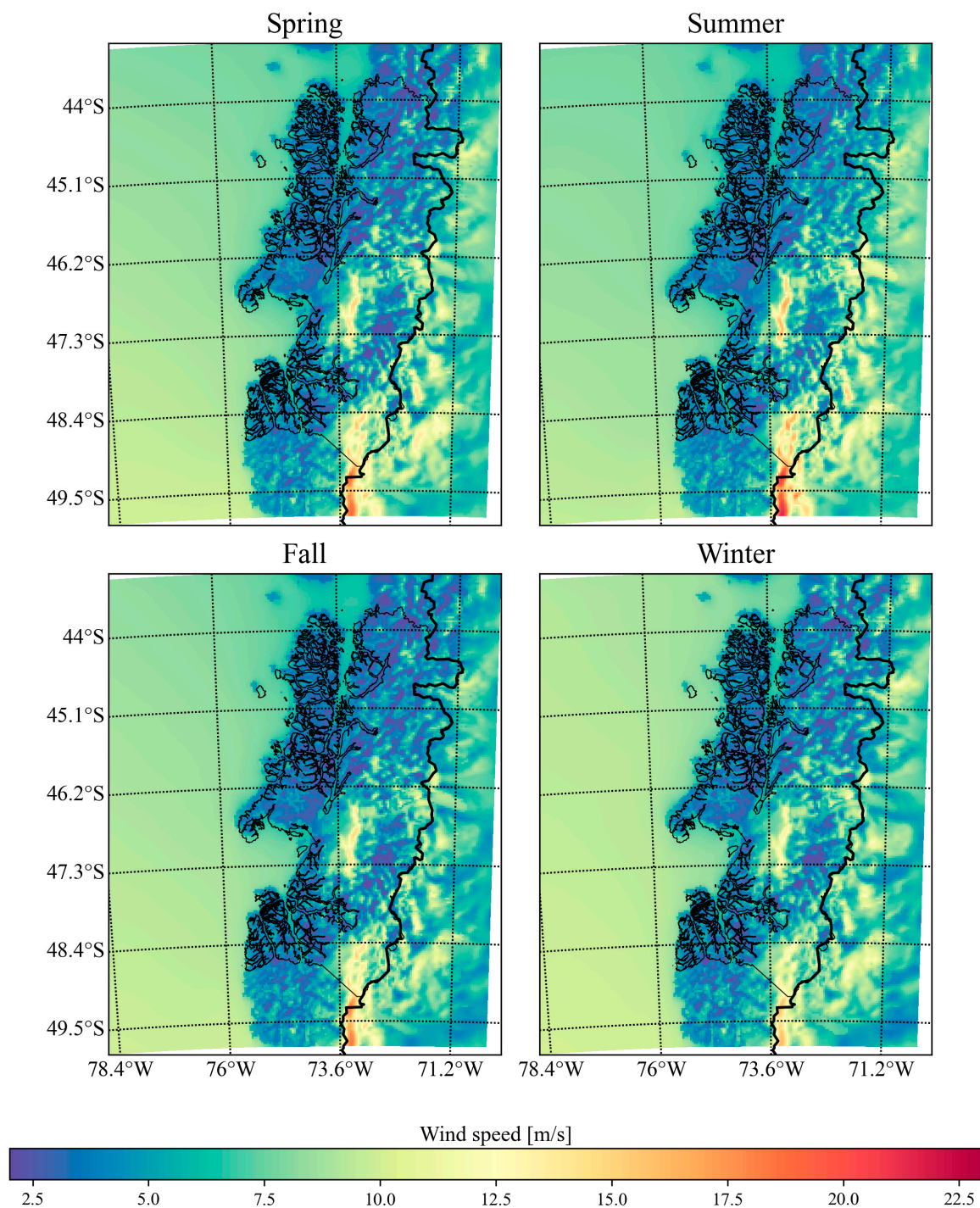
At the Islas las Huichas station, the wind distribution presented the same range of wind speed ( $0\text{--}10 \text{ m s}^{-1}$ ) for all data sets, although there was a difference at  $5 \text{ m s}^{-1}$  where the observation presented a maximum of 10% and the rest of all the data sets had values of higher than 14% in the probability of occurrence. It is important to note that the wind speed observations higher than  $10 \text{ m s}^{-1}$  gathered more than 20% of the wind speed values, and the rest of the data sets decreased the probability of occurrence for wind speeds higher than  $10 \text{ m s}^{-1}$ . At the Melinka Repollal station, there was a clear fit between the MERRA-2 reanalysis and the observations in relation to wind speed distribution for the full range of values, sharing a probability of occurrence of 12% at  $7 \text{ m s}^{-1}$ . Meanwhile, for the other data sets, a decrease in the wind speed was presented in their peak values with higher probabilities of occurrence of over 13%. It is important to note that for wind speed observations exceeding  $10 \text{ m s}^{-1}$ , 15% of data were gathered, while for WRF\_E5 and ERA-5, there were no data. Similarly to Islas las Huichas, the Puesto Viejo station presented the same range of wind speed distribution values ( $0$  to  $10 \text{ m s}^{-1}$ ) for all data sets, although probabilities of occurrence increased to over 11% at  $5 \text{ m s}^{-1}$ , while observations were lower. For this station, 25% of data gathered for wind speed observations were higher than  $10 \text{ m s}^{-1}$ , which is shared by all data sets, except for ERA-5, which only contained 3% of data.

Figure 3 shows a comparison of the Weibull probability density function (PDF) and histograms of wind speed at different measurement sites between the observations, WRF\_E5, RECON80-17 and reanalysis data (ERA-5 and MERRA-2) during the available time period for each station.





**Figure 2.** Weibull PDF curves and histograms for wind speed at all the stations (OBS—black) for WRF\_E5 (red), ERA-5 (orange), MERRA-2 (blue) and RECON80-17 (green).



**Figure 3.** Average seasonal wind speed field map via WRF\_E5 in study area. Summer was defined as December, January and February; winter as June, July and August; fall as March, April and May; and spring as September, October and November.

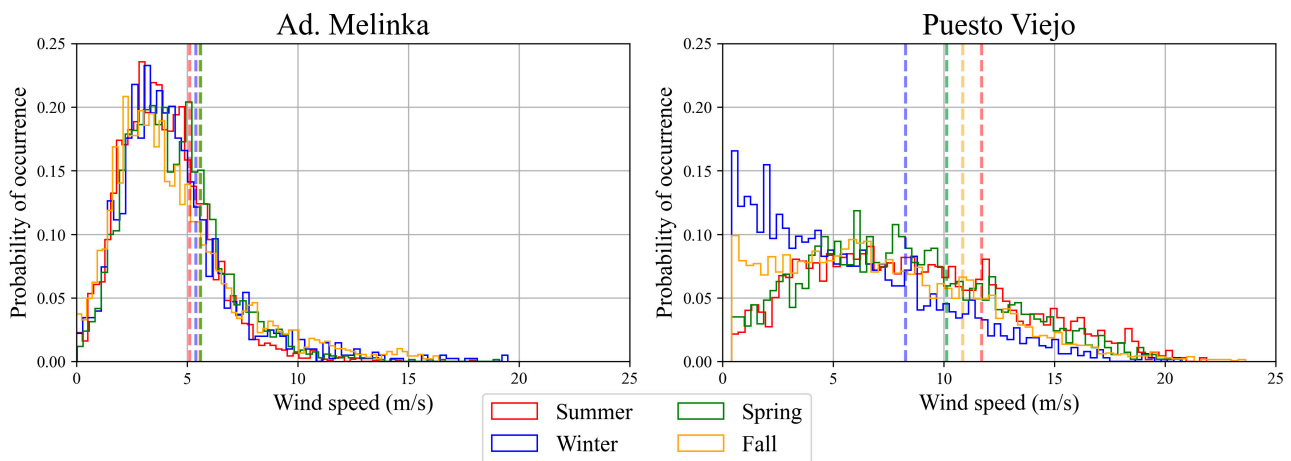
#### 4.2. Seasonal Comparison of Wind Speed from ERA-5, MERRA-2 and WRF\_E5 Data Sets

Figure 3 shows the average seasonal wind speed field map obtained via WRF\_E5 for the study area.

The offshore wind fields are characterized by stable and homogeneous magnitudes during the seasons with an average wind speed of  $9 \text{ m s}^{-1}$ . The wind speed fields gradually increase from north to south, creating a latitudinal gradient that ranges from  $8 \text{ m s}^{-1}$  in the north to  $10 \text{ m s}^{-1}$  in the south. This gradient may be attributed to the persistent influence

of large-scale atmospheric systems such as the South Pacific Anticyclone and the Southern Westerlies, which has also been described in [26]. In addition, the maximum wind speed values are found in the Northern and Southern Patagonian Ice Fields with significantly high values, reaching up to 14 and 20  $\text{m s}^{-1}$ , respectively. These high wind speeds correctly indicate the influence of topography, as the mountain ranges in these areas act as a barrier to the flow of air, causing it to accelerate as it passes through gaps and valleys such as the ice fields. Furthermore, on the Argentinian side, the plains present relatively uniform wind fields with values ranging from 5 to 9  $\text{m s}^{-1}$ , since these terrains are characterized by valleys and open areas.

Figure 4 presents a comparison of wind speed distributions for the four seasons in two measurement stations. In the case of Ad. Melinka, a slight variation in the wind distribution could be observed, which could be attributed to the regulating effect of the nearby sea. This effect reduces the thermal amplitude and consequently limits the extreme differences in seasonal winds. On the other hand, Puesto Viejo exhibited a more pronounced variation, characterized by stronger winds in summer and spring and weaker winds in autumn and winter. These variations could be attributed to influences from local topography and atmospheric conditions specific to the valley, which are more seasonally dependent.



**Figure 4.** Seasonal histogram of wind speed for Ad. Melinka and Puesto Viejo station. The dashed lines represent the 75th percentile for each season.

Figure 5 presents the results of the average station EMD and RMSE values for all data sets. It can be noticed that the seasonal metric's variations are slight at the averaged station. In addition, ERA-5 is statistically different to MERRA-2 and WRF-E5 ( $p$ -value  $< 0.05$ ), and MERRA-2 is non-statistically different to WRF-E5 ( $p$ -value  $> 0.05$ ) for EMD and RMSE. For more details about the seasonal variation in each individual station, see Figure A1 for EMD variation and Figure A2 for PDF Weibull curve variation.

#### 4.3. Comparison of Heat Fluxes at Ñirehuao Station across Different Data Sets

Figure 6 shows energy balance closure analysis and a daily cycle of energy fluxes during the summer in Ñirehuao station. The energy balance closure analysis was performed to evaluate the performance of the EC measurements for the whole experimental duration described in Section 3.1. Regression analysis was performed between hourly data sets of the available energy flux ( $R_n - G$ ) and the turbulent fluxes of consumed energy ( $L + H$ ). The available energy flux was relatively high during the period (summer), with a maximum value of about  $500 \text{ Wm}^{-2}$ , and it was low with a minimum value of about  $-50 \text{ Wm}^{-2}$ . The coefficient of correlation was  $R = 0.942$ , and the regression slope was 1.09.

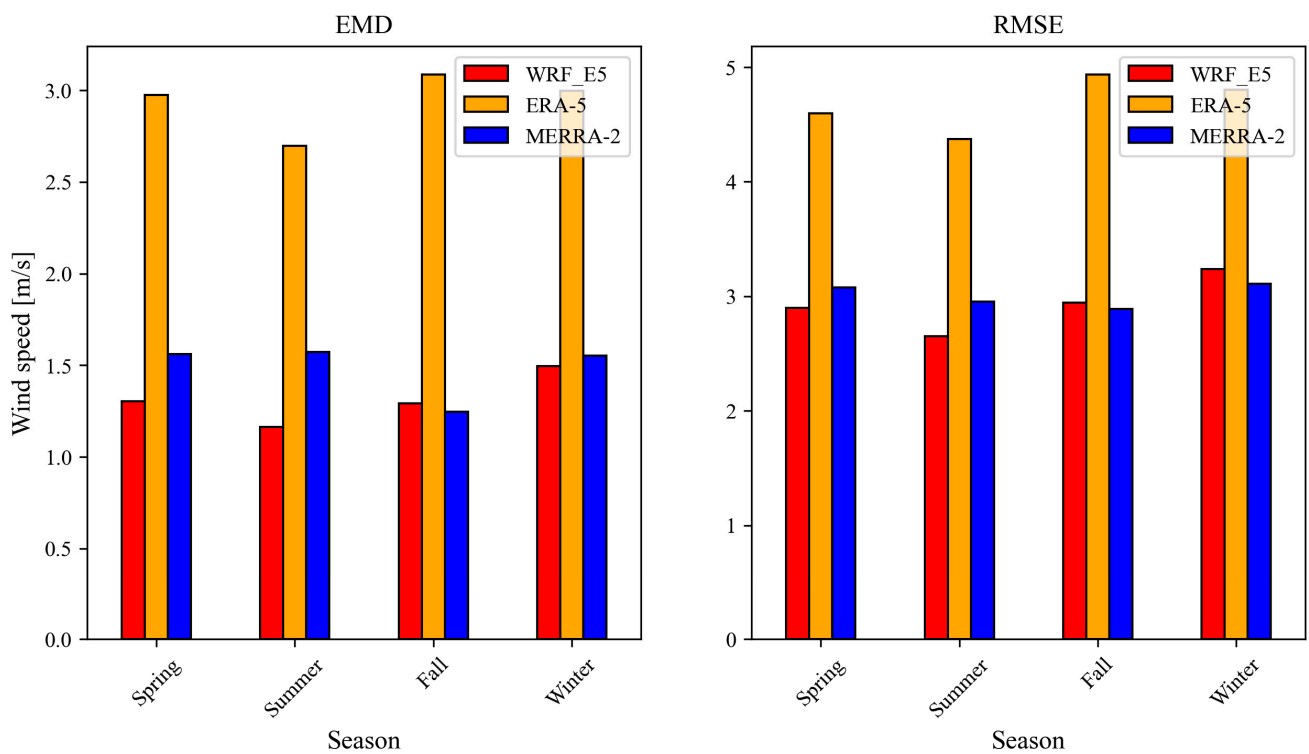


Figure 5. Bar plot of seasonal values of EMD and RMSE for WRF\_E5, ERA-5 and MERRA-2.

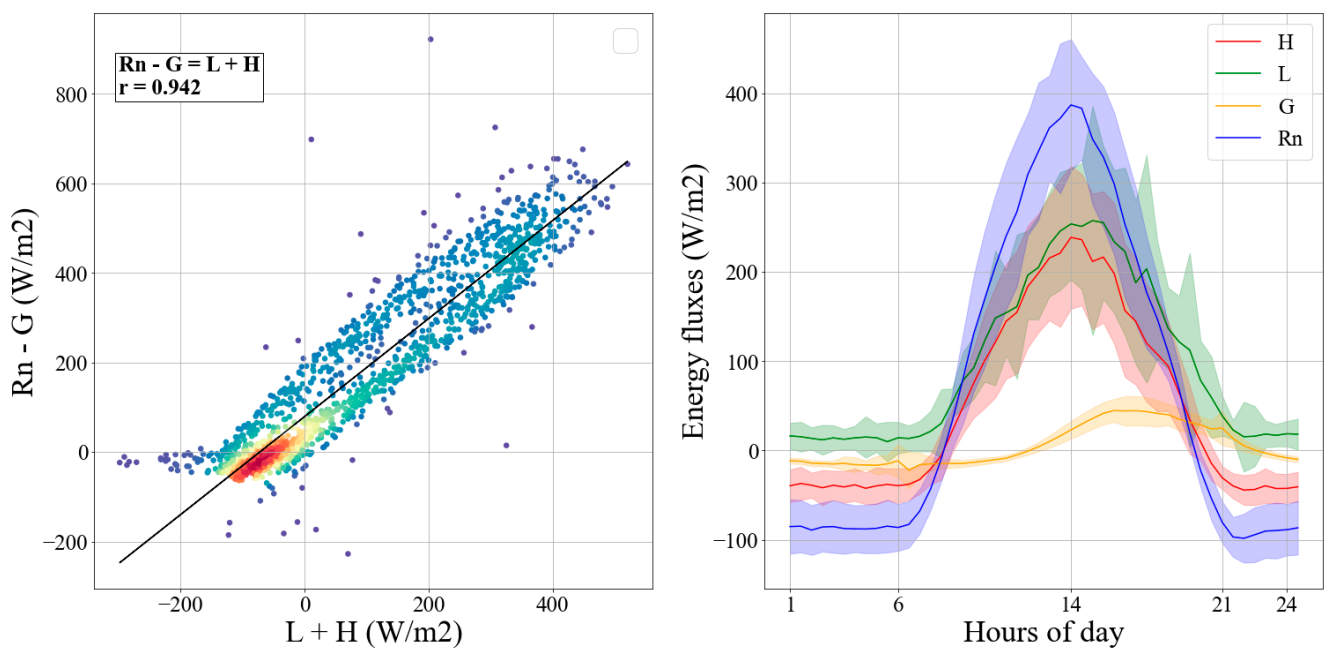
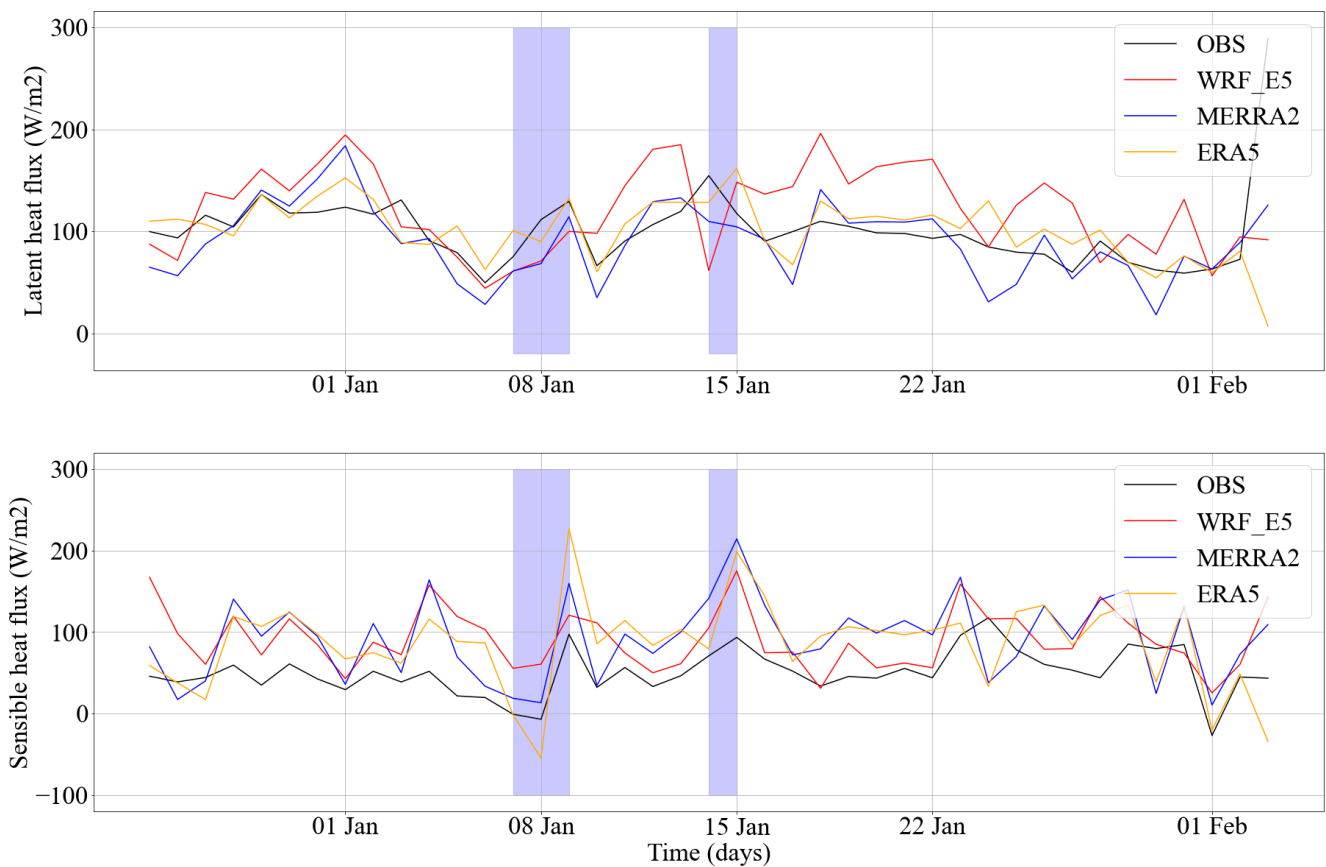


Figure 6. Energy balance closure analysis in the left and daily cycle of energy fluxes in the right. In the left panel, the color gradient represents the density of overlapping data points.

In Figure 7, it can be observed that there was a high increase in sensible heat fluxes from 8 to 15 January. This was related to a warming process that occurred before a rainfall event, which accumulated a great volume of water and clouds during the previous few days (Figure A3). During the rainfall event that occurred on 14 January, the sensible heat fluxes of the data sets were in accordance with observations, having a direct correlation, while the latent heat fluxes at this point were not in accordance with observations. Despite this effect, the comparison of sensible heat fluxes across all data sets appeared to be

in agreement with observations at the station, as they represented the daily variation through time.



**Figure 7.** Latent (**up**) and sensible (**down**) heat fluxes daily time series for WRF\_E5, MERRA-2 and ERA-5 reanalysis at Ñirehuao station. The blue shaded area corresponds to rainfall events.

## 5. Discussion

The findings of this study contribute to a better understanding of the accuracy and limitations of the data sets used in representing wind patterns in WP, since there are no previous studies that specifically compared the RECON80-17 climatological reconstruction with reanalysis tools or NWP from WRF model simulations in this study area. In this work, the comparison between WRF\_E5 and RECON80-17 stated the statistical relation was the best option for representing the wind patterns in WP due to its lowest errors for the years prior to 2017. These results may be attributed to the capability of this model to describe, in a better way, the topography and local conditions of this area due to its finer spatial resolution. Although the RECON80-17 product provides valuable climatological data, it may be necessary to update it in terms of its time coverage (until date) in order to gain a better understanding of its performance and to facilitate comparisons with other stations.

The comparison of MERRA-2 and ERA-5 found that MERRA-2 outperformed ERA-5 in modeling wind speeds, despite its coarser spatial resolution. In fact, MERRA-2 exhibited superior accuracy compared to even WRF\_E5 and RECON80-17 in some cases. However, these findings are not consistent with previous studies in the literature. For example, [12,13,27] have all demonstrated that ERA-5 outperforms other global and regional data sets, including MERRA-2, regional reanalysis and NWP simulations, in assessing wind resources over both flat and sea-level sites with mostly homogeneous land cover, as well as over areas with complex terrain characterized by forest and mountains. In Mexico, [28] also found that ERA-5 performed better than MERRA-2, even in areas with complex topography. Ref. [20] conducted a study evaluating the wind resources at the Cerro Castillo

measurement station (51.17° S, 72.43° W) in Southwestern Patagonia, Chile, and found that ERA-5 slightly outperformed MERRA-2. The study demonstrated that both data sets could reasonably estimate wind speed variability in the region, with a correlation coefficient of over 80% and root mean square errors of 2.7 and 1.9 for MERRA-2 and ERA-5, respectively. These findings suggest that the accuracy of the two reanalysis data sets may depend on the specific region and the characteristics of the terrain and land cover.

The analysis of the flux tower data at Ñirehuao station revealed that ERA-5 struggles to accurately represent certain variables, particularly latent heat fluxes, which exhibited anomalies in the data. This may explain the subpar performance of ERA-5 in modeling wind field patterns at this site, as it serves as a driving force for these patterns [29] have previously noted that ERA-5 tends to perform poorly in predicting wind speeds in regions with significant variations in solar irradiance, such as coastal and mountainous areas, which is the case in WP. Therefore, it is necessary to consider the use of higher-resolution regional reanalysis products or numerical weather prediction models, especially when considering factors such as topography and land use [12].

It is important to note that these studies have also identified limitations in terms of the conditions under which ERA-5 and MERRA2 can be used effectively. In addition to complex terrain, coastal regions present challenges for wind resource estimation due to complex flow regimes caused by surface discontinuities at coastlines. These discontinuities can cause variations in surface roughness and temperature, leading to non-equilibrium wind profiles and unique physical phenomena that complicate forecasting [30]. Additional challenges include land use and forest cover effects on wind flow, as studied by [12,31]. Therefore, as shown in this work, the WRF-E5 simulation is needed to generate a climatology based on ERA-5 reanalysis over Western Patagonia, and the same can be said for MERRA-2 by using the accepted statistical reconstruction for improved performance.

Although the meteorological stations used in this work represent vast areas of WP, covering different configurations of the landscape, further research may be needed to assess the performance of these data sets for both on- and offshore areas. However, the lack of wind measurements at sea surfaces remains a problem for validating wind resource data sets over the study area. Thus, it is important to expand the analysis beyond onshore areas by promoting field campaigns in sea areas for the incorporation of offshore wind resource assessment. Meanwhile, for most onshore measurement sites, reanalysis provides the exact height of the mast towers, so there is no need to use a vertical extrapolation method to equalize the height of time series. This is beneficial because such methods can introduce errors, even in offshore conditions [25]. However, at the Puesto Viejo, Melinka Repollal and Islas Las Huichas mast towers, a vertical extrapolation method was necessary to equalize the heights since most data sets provided wind time series at 10 m. Additionally, when assessing the wind resource, it is necessary to use a vertical extrapolation method to account for the modern wind turbines that have led to hub heights regularly reaching above 60 m onshore [32] and between 70 and 120 m offshore [33], much higher than the installed measurement stations in the study area with the universally standard meteorological measurement height (10 m). These limitations may have an impact on the findings since most of the vertical extrapolation methods adopt stability in the wind vertical profile as an assumption.

Another limitation has been found in the land use model used for WRF\_E5. Several studies have demonstrated the use of a high-resolution land use model improve the performance of NWP simulations over complex terrains. For instance, ref. [34] explored the impact of different land use data sets on simulations using the WRF model in a complex topography zone. They found that the number of categories in the data sets, such as USGS, MODIS and CLC, had an impact on the performance of the simulations. Ref. [35] performed a sensibility analysis comparing different land use data and land surface models, finding that NUL is more consistent in capturing some coverage types such as urban, forest and cropland than USGS land use data. Since higher-resolution land use models enable the effects of the surface layer on wind patterns to be captured, such as sea-land breezes,

speed ups and land–sea discontinuities, it is necessary to use them as part of the WRF model configuration.

## 6. Conclusions

In this study, wind characteristics were downscaled from ERA-5 by using the WRF model, and three available wind data sets, RECON80-17 climatological reconstruction, MERRA-2 and ERA-5, were compared with observations from ten towers in Western Patagonia. Various evaluation metrics (including the RMSE and the EMD) were applied to reveal the differences in applicability between these data sets. The RECON80-17 outperformed WRF\_E5 at the three evaluation sites with small differences of about RMSE = 0.5 and EMD = 0.8 ( $\text{m s}^{-1}$ ). The finer spatial resolution could be one reason for its superiority over the NWP simulation (WRF\_E5). The MERRA-2 reanalysis remarkably outperformed ERA-5 with differences of about RMSE = 1.8 and EMD = 1.6 ( $\text{m s}^{-1}$ ), and non-significant differences were found with WRF\_E5 simulation. The WRF-E5 simulation is needed to generate more accurate climatology based on ERA-5 reanalysis over Western Patagonia, although in some cases, MERRA-2 has presented a similar performance to WRF-E5.

**Author Contributions:** Conceptualization, C.M. and H.H.S.; methodology, N.G.A.-d.-L., C.M. and H.H.S.; validation, H.V.A., C.M., N.G.A.-d.-L. and H.H.S.; formal analysis, H.V.A., M.C, N.G.A.-d.-L. and H.H.S.; investigation, H.V.A., C.M., N.G.A.-d.-L. and H.H.S.; data curation, H.V.A., N.G.A.-d.-L. and J.C.; writing—original draft preparation, H.V.A.; writing—review and editing, H.V.A., C.M., N.G.A.-d.-L. and H.H.S.; visualization, H.V.A. and N.G.A.-d.-L.; supervision, C.M., H.H.S. and N.G.A.-d.-L.; project administration, H.H.S. and C.M. All authors contribute equally. All authors have read and agreed to the published version of the manuscript.

**Funding:** This research was supported as a part of the Fondecyt Regular—Project Code Ref 1211230 awarded to Sepúlveda, H.H. and funded by The Comisión Nacional de Investigación Científica y Tecnológica (Conicyt) de Chile.

**Institutional Review Board Statement:** Not applicable.

**Informed Consent Statement:** Not applicable.

**Data Availability Statement:** Not applicable.

**Acknowledgments:** The authors would like to thank Rodrigo Fuster for his support at the Eddy Covariance Station.

**Powered@NLHPC:** This research was partially supported by the supercomputing infrastructure of the NLHPC (ECM-02).

**Conflicts of Interest:** The authors declare no conflict of interest.

## Abbreviations

The following abbreviations are used in this manuscript:

EC	Eddy Covariance
GFS	Global Forecast System
GLDS	Global Land Data Assimilation System
LSM	Land surface model
LWR	Longwave radiation
NWP	Numerical weather prediction
PBL	Planetary boundary layer
SL	Surface layer
SWR	Shortwave radiation
WRF	Weather Research and Forecasting
WP	Western Patagonia

Appendix A

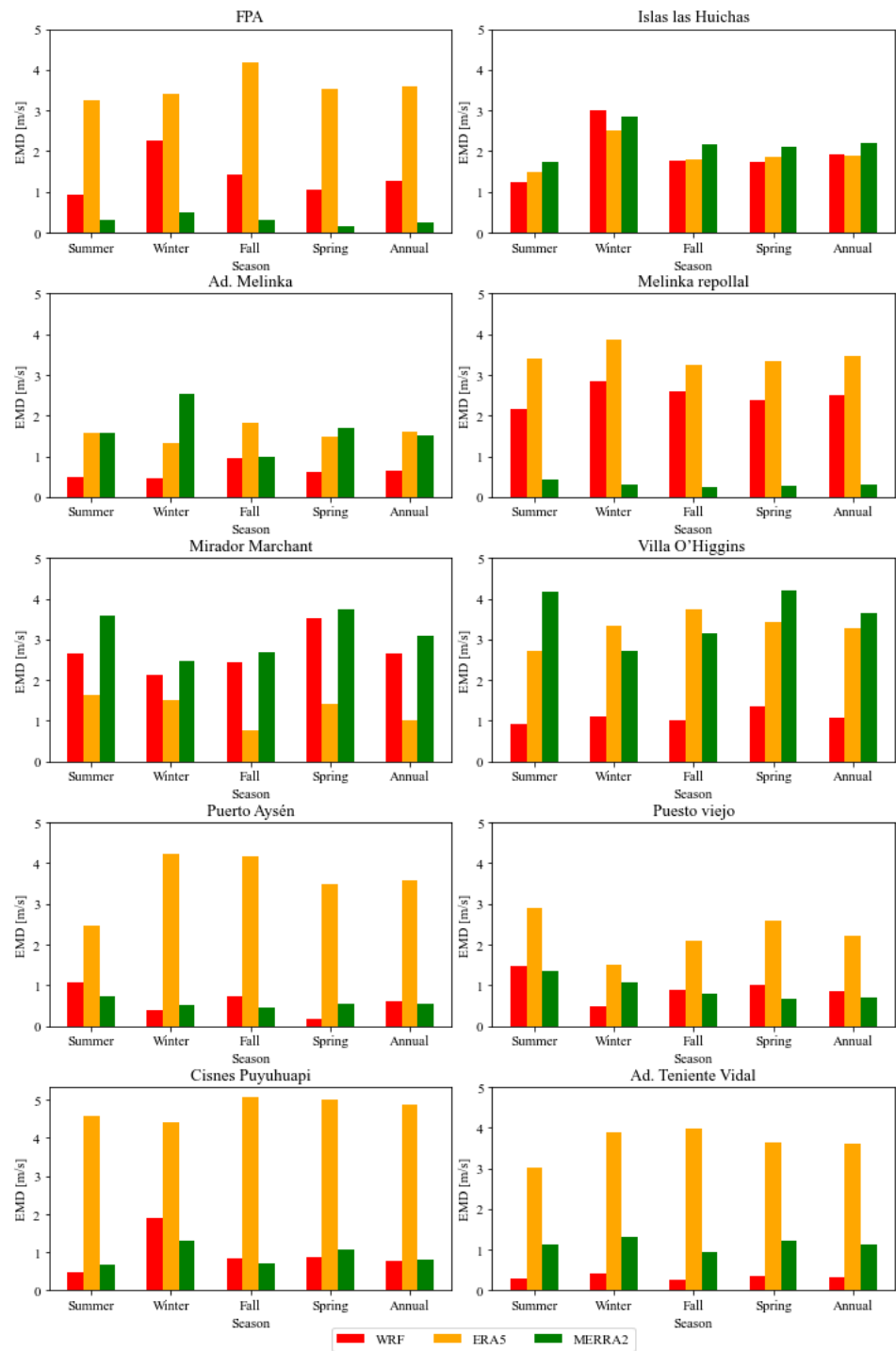


Figure A1. Seasonal and annual comparison of EMD for all measurement stations.



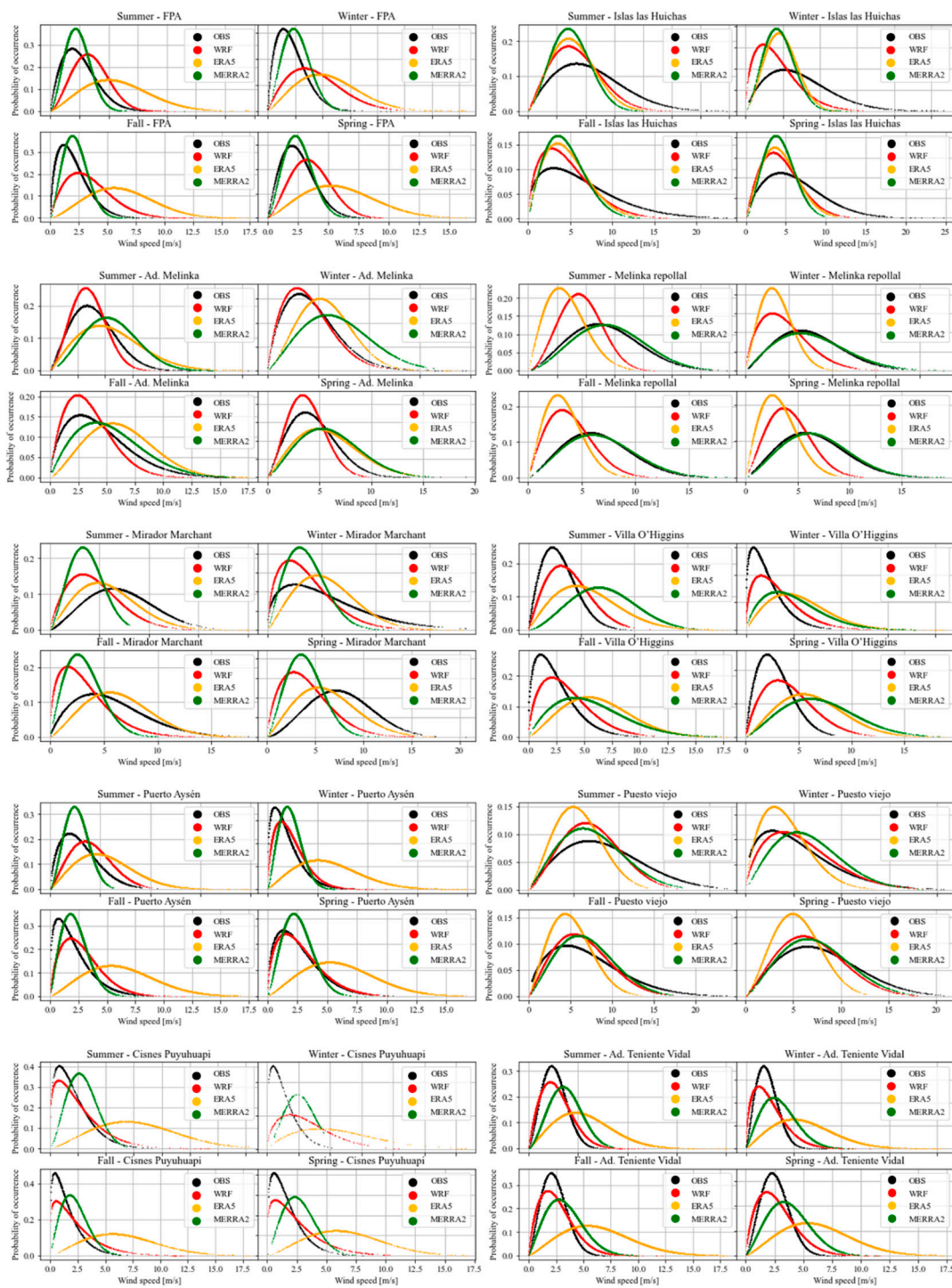


Figure A2. Seasonal comparison of PDF curves for all measurement stations.

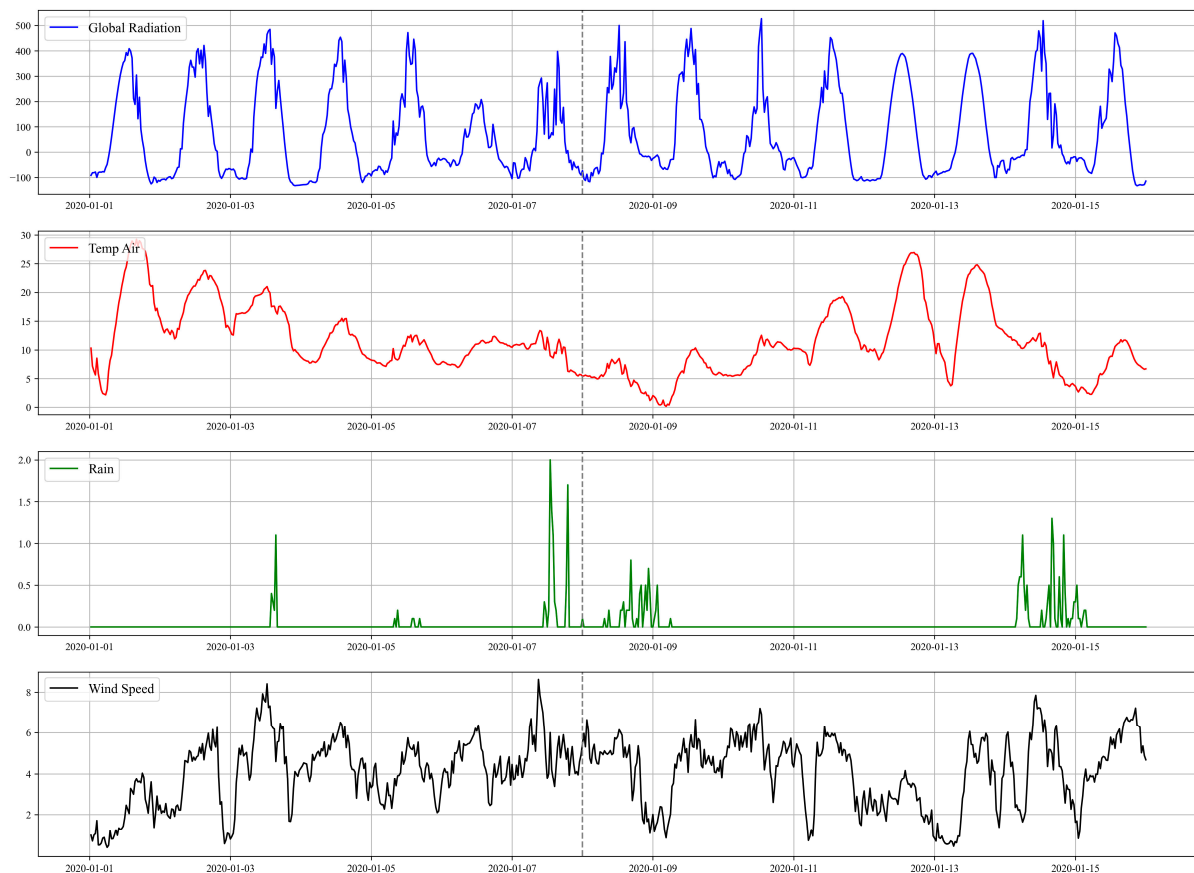


Figure A3. Atmospheric variables at Ñirehuao station during the study period.

## References

- Martínez-Harms, M.J.; Gajardo, R. Ecosystem value in the Western Patagonia projected areas. *J. Nat. Conserv.* **2008**, *16*, 72–87. [[CrossRef](#)]
- Olivera-Guerra, L.; Quintanilla, M.; Moletto-Lobos, I.; Pichuante, E.; Zamorano-Elgueta, C.; Mattar, C. Water dynamics over a Western Patagonian watershed: Land surface changes and human factors. *Sci. Total Environ.* **2022**, *804*, 150221. [[CrossRef](#)] [[PubMed](#)]
- Pérez, T.; Mattar, C.; Fuster, R. Decrease in Snow Cover over the Aysén River Catchment in Patagonia, Chile. *Water* **2018**, *10*, 619. [[CrossRef](#)]
- Olivares-Contreras, V.; Mattar, C.; Gutiérrez, A.; Jiménez, J. Warming trends in Patagonian subantarctic forest. *Int. J. Appl. Earth Obs. Geoinf.* **2019**, *76*, 51–65. [[CrossRef](#)]
- Mattar, C.; Borvarán, D. Off-shore wind power simulation by using WRF in the central coast of Chile. *Renew. Energy* **2016**, *94*, 22–31. [[CrossRef](#)]
- Muñoz, R.C.; Falvey, M.J.; Arancibia, M.; Astudillo, V.I.; Elgueta, J.; Ibarra, M.; Santana, C.; Vásquez, C. Wind Energy Exploration over the Atacama Desert: A Numerical Model-Guided Observational Program. *Bull. Am. Meteorol. Soc.* **2018**, *99*, 2079–2092. [[CrossRef](#)]
- De Linaje, N.G.-A.; Mattar, C.; Borvarán, D. Quantifying the wind energy potential differences using different WRF initial conditions on Mediterranean coast of Chile. *Energy* **2019**, *188*, 116027. [[CrossRef](#)]
- Brune, S.; Keller, J.D.; Wahl, S. Evaluation of wind speed estimates in reanalyses for wind energy applications. *Adv. Sci. Res.* **2021**, *18*, 115–126. [[CrossRef](#)]
- Hasager, C.B.; Hahmann, A.N.; Ahsbahs, T.; Karagali, I.; Sile, T.; Badger, M.; Mann, J. Europe's offshore winds assessed with synthetic aperture radar, ASCAT and WRF. *Wind Energy Sci.* **2020**, *5*, 375–390. [[CrossRef](#)]
- Dörenkämper, M.; Olsen, B.T.; Witha, B.; Hahmann, A.N.; Davis, N.N.; Barcons, J.; Ezber, Y.; García-Bustamante, E.; González-Rouco, J.F.; Navarro, J.; et al. The Making of the New European Wind Atlas—Part 2: Production and evaluation. *Geosci. Model Dev.* **2020**, *13*, 5079–5102. [[CrossRef](#)]
- Li, H.; Claremar, B.; Wu, L.; Hallgren, C.; Körnich, H.; Ivanell, S.; Sahlée, E. A sensitivity study of the WRF model in offshore wind modeling over the Baltic Sea. *Geosci. Front.* **2021**, *12*, 101229. [[CrossRef](#)]
- Gualtieri, G. Reliability of ERA5 Reanalysis Data for Wind Resource Assessment: A Comparison against Tall Towers. *Energies* **2021**, *14*, 4169. [[CrossRef](#)]

13. Olauson, J. ERA5: The new champion of wind power modelling? *Renew Energy* **2018**, *126*, 322–331. [[CrossRef](#)]
14. Dorrego Portela, J.R.; Hernández Galvez, G.; Hernandez-Escobedo, Q.; Saldaña Flores, R.; Sarracino Martínez, O.; Lastres Danguillecourt, O.; López de Paz, P.; Perea-Moreno, A.-J. Microscale Wind Assessment, Comparing Mesoscale Information and Observed Wind Data. *Sustainability* **2022**, *14*, 11991. [[CrossRef](#)]
15. Carvalho, D. An Assessment of NASA's GMAO MERRA-2 Reanalysis Surface Winds. *J. Clim.* **2019**, *32*, 8261–8281. [[CrossRef](#)]
16. Carvalho, D.; Rocha, A.; Gómez Gesteira, M.; Santos, C.S. WRF wind simulation and wind energy production estimates forced by different reanalyses: Comparison with observed data for Portugal. *Appl. Energy* **2014**, *117*, 116–126. [[CrossRef](#)]
17. Staffell, I.; Pfenninger, S. Using bias-corrected reanalysis to simulate current and future wind power output. *Energy* **2016**, *114*, 1224–1239. [[CrossRef](#)]
18. Zhou, Y.; Mu, Z. Impact of Different Reanalysis Data and Parameterization Schemes on WRF Dynamic Downscaling in the Ili Region. *Water* **2018**, *10*, 1729. [[CrossRef](#)]
19. Tavares, L.F.D.A.; Shadman, M.; Assad, L.P.D.F.; Estefen, S.F. Influence of the WRF model and atmospheric reanalysis on the offshore wind resource potential and cost estimation: A case study for Rio de Janeiro State. *Energy* **2021**, *240*, 122767. [[CrossRef](#)]
20. Gómez-Fontalba, C.; Flores-Aqueveque, V.; Alfaro, S.C. Variability of the Southwestern Patagonia (51°S) Winds in the Recent (1980–2020) Period: Implications for Past Wind Reconstructions. *Atmosphere* **2022**, *13*, 206. [[CrossRef](#)]
21. Skamarock, W.C.; Klemp, J.B.; Dudhia, J.; Gill, D.O.; Barker, D.M.; Duda, M.G.; Huang, X.-Y.; Wang, W.; Powers, J.G. *A Description of the Advanced Research WRF Version 3*; NCAR Technical: Boulder, CO, USA, 2008; p. 113. [[CrossRef](#)]
22. Hahmann, A.N.; Sile, T.; Witha, B.; Davis, N.N.; Dörenkämper, M.; Ezber, Y.; García-Bustamante, E.; González-Rouco, J.F.; Navarro, J.; Olsen, B.T.; et al. The making of the New European Wind Atlas—Part 1: Model sensitivity. *Geosci. Model Dev.* **2020**, *13*, 5053–5078. [[CrossRef](#)]
23. Hahmann, A.N.; Lennard, C.; Badger, J.; Vincent, C.L.; Kelly, M.C.; Volker, P.J.; Argent, B.; Refslund, J. Mesoscale modeling for the Wind Atlas of South Africa (WASA) project. *DTU Wind Energy* **2015**, *50*, 80.
24. Peleg, S.; Werman, M.; Rom, H. A unified approach to the change of resolution: Space and gray-level. *IEEE Trans. Pattern Anal. Mach. Intell.* **1989**, *11*, 739–742. [[CrossRef](#)]
25. Optis, M.; Bodini, N.; Debnath, M.; Doubrawa, P. *Best Practices for the Validation of U.S. Offshore Wind Resource Models*; NREL/TP-5000-78375; National Renewable Energy Laboratory: Golden, CO, USA, 2020.
26. Garreaud, R.; Lopez, P.; Minvielle, M.; Rojas, M. Large Scale Control on the Patagonian Climate. *J. Clim.* **2013**, *26*, 215–230. [[CrossRef](#)]
27. Jourdiier, B. Evaluation of ERA5, MERRA-2, COSMO-REA6, NEWA and AROME to simulate wind power production over France. *Adv. Sci. Res.* **2020**, *17*, 63–77. [[CrossRef](#)]
28. Thomas SH, L.; Nicolau, S.; Martinez-Alvarado, O.; Drew, D.S.; Bloomfield, H. How well do atmospheric reanalyses reproduce observed winds in coastal regions of Mexico? *Meteorol. Appl.* **2021**, *28*, e2023. [[CrossRef](#)]
29. Urraca, R.; Huld, T.; Gracia-Amillo, A.; Martinez-De-Pison, F.J.; Kaspar, F.; Sanz-Garcia, A. Evaluation of global horizontal irradiance estimates from ERA5 and COSMO-REA6 reanalyses using ground and satellite-based data. *Sol. Energy* **2018**, *164*, 339–354. [[CrossRef](#)]
30. Dörenkämper, M.; Optis, M.; Monahan, A.; Steinfeld, G.; Doerenkaemper, M. On the Offshore Advection of Boundary-Layer Structures and the Influence on Offshore Wind Conditions. *Bound.-Layer Meteorol.* **2015**, *155*, 459–482. [[CrossRef](#)]
31. Lydia, M.; Kumar, S.S.; Selvakumar, A.I.; Kumar, G.E.P. Wind resource estimation using wind speed and power curve models. *Renew. Energy* **2015**, *83*, 425–434. [[CrossRef](#)]
32. Gualtieri, G. Improving investigation of wind turbine optimal site matching through the self-organizing maps. *Energy Convers. Manag.* **2017**, *143*, 295–311. [[CrossRef](#)]
33. Soares, P.; Lima DC, A.; Cardoso, R.M.; Nascimento, M.L.; Semedo, A. Western Iberian offshore wind resources: More or less in a global warming climate? *Appl. Energy* **2017**, *203*, 72–90. [[CrossRef](#)]
34. Golzio, A.; Ferrarese, S.; Cassardo, C.; Diolaiuti, G.A.; Pelfini, M. Land-Use Improvements in the Weather Research and Forecasting Model over Complex Mountainous Terrain and Comparison of Different Grid Sizes. *Bound.-Layer Meteorol.* **2021**, *180*, 319–351. [[CrossRef](#)]
35. Teklay, A.; Dile, Y.T.; Asfaw, D.H.; Bayabil, H.K.; Sisay, K. Impacts of Land Surface Model and Land Use Data on WRF Model Simulations of Rainfall and Temperature over Lake Tana Basin, Ethiopia. *Heliyon* **2019**, *5*, e02469. [[CrossRef](#)] [[PubMed](#)]

**Disclaimer/Publisher's Note:** The statements, opinions and data contained in all publications are solely those of the individual author(s) and contributor(s) and not of MDPI and/or the editor(s). MDPI and/or the editor(s) disclaim responsibility for any injury to people or property resulting from any ideas, methods, instructions or products referred to in the content.